Lattice modelling of hydraulic fracture: theoretical validation and interactions with cohesive joints

Vincent Lefort, Olivier Nouailletas, David Grégoire, Gilles Pijaudier-Cabot

Version of Record: https://www.sciencedirect.com/science/article/pii/S001379442030761X
Manuscript_d9f339feb1ecba1c3bd7f35bc84609b6

Lattice modelling of hydraulic fracture: theoretical validation and interactions with cohesive joints

Vincent Lefort[a], Olivier Nouailletas[a], David Grégoire[a,b], Gilles Pijaudier-Cabot[a,b,*]

[a] *Universite de Pau et des Pays de l'Adour, E2S UPPA, CNRS, Total, LFCR, Allée du Parc Montaury, F-64600 Anglet, France*
[b] *Institut Universitaire de France, Paris, France*

Abstract

A hydro-mechanical coupled lattice-based model for the simulation of crack propagation induced by fluid injection in porous saturated rocks containing cohesive joints is presented. Rock follows an isotropic damage model for tensile fracture and cohesive joints follow a coupled plasticity-damage model. The discretisation uses a dual lattice approach: a Delaunay triangulation for the solid and the boundaries of the associated Voronoï tesselation for the hydraulic part. A classical poromechanical framework for a materials saturated with a single fluid is implemented. First, predictions of crack propagation are compared with analytical models. Then, the interaction between a propagating crack and an existing joint is analysed. Two configurations are considered: the case of a joint that is orthogonal to the crack path and the case of a joint that is inclined by 45^o with respect to the crack path. For the vertical joint, the crack is first arrested because the cohesive joint is weaker than the rock mass. The crack reinitiates at both crack tips and subsequently propagates in one of them. For the inclined joint, the crack follows the joint and therefore its path is deviated. Damage in the rock develops in the back of the crack tip, thereby enhancing the increase of permeability due to damage in the rock mass.

Keywords:
Damage, Lattice, Hydromechanical coupling, Plastic-damageable joint

1. Introduction

Hydraulically-driven crack propagation is a complex problem with various applications ranging from magma transport in the lithosphere (dikes, see e.g. Ref. [36]), oil and gas reservoir stimulation [13], to dam safety analyses [47] and geological nuclear waste repository as well.

In the case of a hydraulically-driven crack in a homogeneous material, different analytical solutions are available, dealing with the so-called bi-wing configuration, the case of two cracks

*Corresponding author
Email address: Gilles.Pijaudier-Cabot@univ-pau.fr (Gilles Pijaudier-Cabot)

propagating at both tips of an existing one. For the KGD[1] configuration, see e.g. the results in Refs. [29] or [17]; for the PKN[2] configuration, see e.g. the contributions in Refs. [42], [40] or [1]; for a comparison of the two, see Ref. [18]. These analytical solutions predict the width and extend of hydraulically-induced fractures by taking into account the fluid transfer within the matrix through a Carter's *leak-off* coefficient [28] but to solve the problem analytically, different asymptotic regimes are distinguished. The fluid flow may be dominated by the leak-off or the fluid may preferentially be stored within the propagating crack. The mechanical energy may be preferentially dissipated through the matrix fracture (toughness-dominated) or through frictional shear forces within the fluid (viscosity-dominated) (see for instance Ref. [5], for a study of a toughness-dominated hydraulic fracture with leak-off). For intermediate cases, the model cannot be solved analytically and numerical modeling is needed.

Several computational models for the simulation of hydraulic fracturing are available in the literature, see e.g. the recent review by Lecampion and co-workers [32] and also the review by Hattori and co-workers [25] in the context of shale gas production. For instance, standard Galerkin finite elements with remeshing, central force models and the extended finite element method have been used by Cao and co-workers [6]. Central force (lattice) models have been used starting in the 90's for the purpose of simulating hydraulic fracture in homogeneous and heterogeneous media. In Ref. [48] dry and fully saturated conditions (using Biot Theory) have been considered, with a view to the correlations involved in crack propagation and to the microseismicity that is induced. More recently, Milanese and co-workers [37, 38] looked at similar issues and investigated the pressure oscillations and their correlation during hydraulic fracturing under mode I and mixed mode conditions. Central force model are based on networks of trusses [37, 38], beams [39, 22], or nonlinear springs placed between rigid bodies [3, 41] generated with the help of Delaunay triangulation or granular packing. The hydraulic problem is described either by solving the stoke equation in the pore network [41] or by considering a dual lattice discrete problem [48]. Dual lattice approaches for solving the hydro-mechanical coupled problem have been also used by Chatzigeorgiou at al. [8] for studying how damage and permeability should be coupled in a continuum context, and further implemented in a wide variety of analyses dealing with poromechanics in saturated and unsaturated rocks (see e.g. [34, 2]). In addition to the correlations involved during fracture propagation and to the influence of the fluid on these correlations mentioned above, various effects have been also studied, such as the interaction between different stimulated cracks [31, 46], or the influence of the spatial variation of the rock mechanical properties on the crack extensions [30]. Also, the influence of the host rock anisotropy may induce crack branching and change crack spacing due to the contrast of permeability properties [43, 9].

The mechanical and hydraulic behaviour of a rock formation is often dominated by a network of pre-existing joints. This is particularly the case for source rocks, which have been intensively fractured hydraulically for oil and gas extraction (see e.g. Ref. [16], for a description of natural fractures in Barnett shales). Natural joints may have been cemented

[1] Kristonovich-Geertsma-de Klerk

[2] Perkins-Kern-Nordgren

by geological fluid flows and the global permeability of the system will highly depend on the capacity of the hydraulic fracture to reactivate these natural joints. In addition to the complexity of models that involve fluid-porous skeleton interactions and fluid flow in fracture, the mechanical response of these joints and their degradation due to fluid pressure ought to be addressed for such a purpose. Most existing models for this rely on (i) a description of the fracture propagation, e.g. according to a cohesive crack model, (ii) an hydrodynamics-based model for the fluid flow in the fracture, and (iii) a geomechanical joint model. An exemple of such a combination is the work due to Fu et al. [15] where adaptative remeshing needs to be implemented in order to follow crack propagation. Multiscale approaches have also been devised for the same purpose. They combine for instance a coarse description that fits large-scale calculations to an extended finite element approach with enriched functions at the lower scale [4, 45]. Recently, analytical derivations of the strain energy release rate involved in crack propagation that deflects upon reaching weak interfaces or involves crack-surface friction and the anisotropy of the crustal stress were also proposed [50]. They agree with the theoretical formulation for a crack tip reaching an interface between dissimilar elastic media [26]. Nevertheless, such variations of the crack propagation conditions have not been implemented in formulations aimed at predicting hydraulic fracture yet.

In this paper we use a lattice-type numerical model allowing the simulation of crack propagation under fluid injection in a quasi-brittle porous heterogeneous medium. This numerical model uses a dual Voronoï/Delaunay description, which is very efficient to represent dual mechanical/hydraulic couplings [19]. The lattice model, being based on continuum damage, has demonstrated in the past its capacity at dealing easily with crack propagation (i.e. the propagation of a damage band in a continuum setting) in heterogeneous media [23, 20, 33]. It provides also an alternative to the phase field approaches for fracture that have been proposed in the literature over the recent years (see e.g. Refs [27, 35]). This computational model will be used here to get a better understanding of initiation and propagation conditions of cracks in rock masses presenting a natural cohesive joint, where the coupling between mechanical damage and fluid transfer properties are at stake.

This contribution follows the initial results summarised in Ref. [24] which will be thoroughly documented along with additional results. It is organized as follows. After having briefly recalled in Section 2 the lattice model used in this paper, we proceed in Section 3 to the comparisons with analytical solutions. Section 4 presents the influence of a cohesive joint of finite length on the propagation of fracture.

2. Lattice modeling

We start here from a 2D plane-stress lattice model that is based on the numerical framework proposed by Grassl and Jirasek [21]. First, the mechanical description is addressed, and then the hydraulic modelling is detailed. The restriction to 2D modelling should not be seen as a limitation of the computational approach that is easily applicable to 3D examples. Rather, it is for the sake of convenience, of computational cost, and also of comparisons with existing analytical results that we limit ourselves to 2D calculations.

The coupled hydro-mechanical response of the material rests upon poromechanics of saturared porous media. It means the effective stress σ^t applied to the solid matrix is related to the applied stress σ and to the variation of pore pressure $p - p_0$ according to the classical relationship [12]:

$$\sigma^t = \sigma - b(p - p_0)[I] \tag{1}$$

where b is the Biot coefficient and $[I]$ is the identity tensor.

2.1. Mechanical description

The solid skeleton of the porous material is supposed to be homogeneous and the lattice is made of beam elements, which idealize the material structure. First, nodes are randomly distributed in the domain, such that a minimum distance is enforced. The lattice elements result then from a Delaunay triangulation (solid lines in figure 1a) and the middle cross-sections of the lattice elements are the edges of the polygons of the dual Voronoi tesselation (dashed lines in figure 1a).

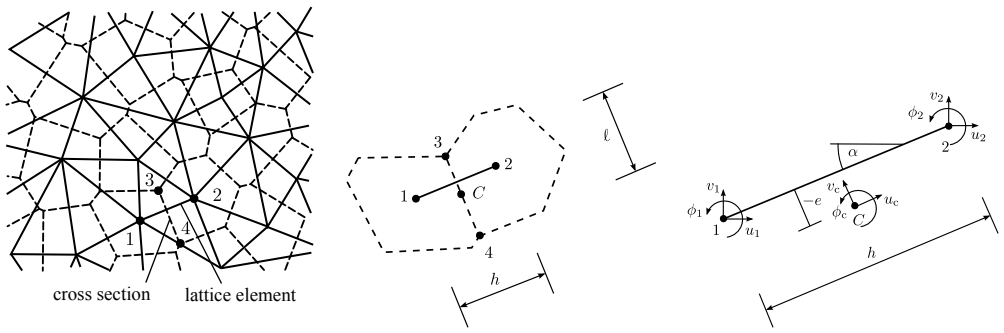

(a) (b) (c)

Figure 1: (1a) Set of lattice elements (solid lines) with middle cross-sections (dashed lines) obtained from the Voronoi tessellation of the domain. (1b) and (1c) Lattice element in the global coordinate system (reproduced from [20]).

Each node has three degrees of freedom (in 2D): two translations (u, v) and one rotation (ϕ) as depicted in figure 1c. In the global coordinate system, the degrees of freedom of nodes 1 and 2, noted $u_e = (u_1, v_1, \phi_1, u_2, v_2, \phi_2)^T$, are related to the displacement jumps in the local coordinate system of point C, $u_c = (u_c, v_c, \phi_c)^T$, see Fig. 1b. u_c is related u_e according to equation 2.

$$u_c = \mathbf{B} u_e \tag{2}$$

where

$$\mathbf{B} = \begin{bmatrix} -\cos\alpha & -\sin\alpha & -e & \cos\alpha & \sin\alpha & e \\ \sin\alpha & -\cos\alpha & -h/2 & \cos\alpha & \sin\alpha & -h/2 \\ 0 & 0 & \sqrt{I/A} & 0 & 0 & -\sqrt{I/A} \end{bmatrix} \tag{3}$$

Point C is located at the center of the middle cross-section of the element as represented in figures 1b and 1c. The matrix $\mathbf{B}$ depends on the orientation α of the element in the global coordinate system, on the distance e between point C and the segment relating nodes 1 and 2, on the distance h between two nodes, and on the element cross-sectional area A and its second moment I (see [20] for details).

The strains $\varepsilon = (\varepsilon_n, \varepsilon_s, \varepsilon_\phi)^T$ associated to the displacement u_c at point C are:

$$\varepsilon = \frac{u_c}{h} = (\varepsilon_n, \varepsilon_s, \varepsilon_\phi)^T \tag{4}$$

The effective stresses $\sigma^t = (\sigma_n^t, \sigma_s^t, \sigma_\phi^t)^T$ are related to the strains ε following the mechanical constitutive relation at the lattice level, here an isotropic damage model to be described further. The subscripts n and s refer to the normal and shear components of the strain and stress vector.

The (secant) stiffness matrix $\mathbf{K}$ of the lattice element is defined as follows:

$$\mathbf{K} = \frac{A}{h}\mathbf{B}^T\mathbf{D}\mathbf{B} \tag{5}$$

where $\mathbf{D}$ is the material stiffness matrix computed at point C.

An isotropic damage model (Eq. 6) is used to describe the mechanical response of the lattice element:

$$\sigma^t = (\sigma_n^t, \sigma_s^t, \sigma_\phi^t)^T = (1-\omega)\mathbf{D}_e\varepsilon = (1-\omega)\overline{\sigma} \tag{6}$$

where ω is the damage variable, $\mathbf{D}_e$ is the elastic stiffness and $\overline{\sigma} = (\bar{\sigma}_\mathrm{n}, \bar{\sigma}_\mathrm{s}, \bar{\sigma}_\phi)^T$ is the true stress in the continuum damage mechanics sense. The elastic stiffness defined as:

$$\mathbf{D}_\mathrm{e} = \begin{bmatrix} E & 0 & 0 \\ 0 & \gamma E & 0 \\ 0 & 0 & E \end{bmatrix} \tag{7}$$

depends on model parameters E and γ, which control Young's modulus and Poisson's ratio of the equivalent continuum. The equivalent strain is then calculated from equation (8) where ε_0, c and q are model parameters.

$$\varepsilon_{eq} = \frac{1}{2}\varepsilon_0(1-c) + \sqrt{\left(\frac{1}{2}\varepsilon_0(c-1) + \varepsilon_n\right)^2 + \frac{c\gamma^2\varepsilon_s^2}{q}} \tag{8}$$

The expression for the damage parameter ω is derived by considering pure tension where the softening curve under monotonically increasing tensile strain is chosen to be of the exponential-type:

$$\sigma_n^t = f_t \exp\left(-\frac{w_{cn}}{w_f}\right) \tag{9}$$

where $w_{cn} = \omega h \varepsilon_n$ is the crack opening, w_f is the initial slope of the softening curve, which is related to the meso-level fracture energy as $G_f = f_t w_f$. This stress-strain law can also be written, for uniaxial tension, as a function of the damage variable as in equation (10).

$$\sigma_n = (1-\omega)E\varepsilon_n \tag{10}$$

In uniaxial tension, the nominal stress is limited by the tensile strength ($f_t = E\varepsilon_0$) and thus, by using these two expressions of σ_n, Eqs. (9,10), one obtains the expression which governs the evolution of the damage variable ω:

$$(1-\omega)\kappa^d = \varepsilon_0 \exp\left(-\frac{\omega h \kappa^d}{w_f}\right) \tag{11}$$

where ε_n has been replaced by κ^d which is the history dependent variable for damage determined by Eq. (12a) with the Kuhn-Tucker loading-unloading conditions (12b):

$$f(\varepsilon, \kappa^d) = \varepsilon_{eq}(\varepsilon) - \kappa^d \tag{12a}$$

$$f \leq 0, \quad \dot{\kappa^d} \geq 0, \quad \dot{\kappa^d} f = 0 \tag{12b}$$

The elastic constants and the model parameters in the damage models are calibrated on a specific material from an inverse analysis technique [20]. In Ref. [24], it has been shown that when the thickness of damage band is sufficiently small, this lattice model compares quite well with results obtained from linear elastic fracture mechanics in the case of a crack loaded by a constant internal pressure. This is the case here because the solid is assumed to be homogeneous and therefore, the width of the damage band cannot result from material heterogeneity. It may result from the local disorder induced by the lattice discretisation only, but upon refinement convergence towards LEFM is recovered.

2.2. Hydraulic description

In the context of clasical poromechanics, we assume that the matrix porosity is connected and its volume depends on the fluid pressure and that the fluid saturates the porous medium. Laminar and incompressible flow is considered and gravity effects are neglected. The porosity and flux density are related following Eq.(13):

$$\frac{\partial \phi}{\partial t} + \mathrm{div}(\vec{q}) = 0 \tag{13}$$

where ϕ is represent the connected porosity (volume of connected porosity divided by total volume of the porous medium), $\vec{q}$ is the volumetric flux density of fluid, and t is time.

Considering Darcy's law, volumetric flux density of fluid is related to fluid pressure gradient:

$$\vec{q} = -k \times \overrightarrow{\mathrm{grad}(\frac{p}{\rho g})} \tag{14}$$

where k is the hydraulic conductivity of the medium (m.s^{-1}), p is the fluid pressure (Pa), ρ is the volumetric mass of the fluid and g is the gravitational acceleration.

In a medium with cracks, hydraulic conductivity can be represented considering two contributions : the first one is the conductivity of the homogeneous matrix, k_0, the second one is the conductivity of cracks k_c. In a homogeneous medium, the hydraulic conductivity k_0 can be deduced from the permeability κ:

$$k = k_0 + k_c = \frac{\rho g}{\mu}\kappa + k_c \tag{15}$$

where μ is the dynamic viscosity of the fluid (Pa.s), and κ is the permeability of the homogeneous medium (m^2). The conductivity of the crack will be discussed in the next section.

The variation of porosity due to the applied effective stress and to the pore pressure is:

$$\phi - \phi_0 = b\varepsilon_V + \frac{p - p_0}{N} \tag{16}$$

where $\phi - \phi_0$ is the variation of porosity, ε_V is the first invariant of the strain tensor (volumetric strain), and N is Biot's modulus. For saturated medium, it is standard to define a modulus M related to N, ϕ_0 and the fluid bulk modulus K_f:

$$\frac{1}{M} = \frac{1}{N} + \frac{\phi_0}{K_f} \tag{17}$$

In the remainder of this paper we consider parameters and validations cases given by [7] : that is to say E=17GPa, $\phi_0 = 0.2$ and M=68.7MPa. With these parameters, in equation (16), $b\varepsilon_V$ is negligible compared to $\frac{p-p_0}{N}$. Hence, the differential equation describing the diffusion of the fluid into the matrix reduces to:

$$\frac{1}{M}\frac{\partial p}{\partial t} - \frac{k}{\rho g}\Delta p = 0 \tag{18}$$

Because the influence of the volumetric strain is neglected in the above equation, the increasing storage capacity of the porous materials upon dilation of the pore space is neglected. This is also true when the material is fully damaged, which means that the storage capacity of the crack is also neglected. Cracking is described with a continuum setting (damage model), and the fluid-solid coupling parameters in the poromechanics approach are set constant, therefore, the same assumption holds for the undamaged and the damaged material as well. Let us stress that this is a limitation of the present analysis which ought to be seen as restricted to the leak-off regime where the fluid flows in the porous material and at the same time induces fracture propagation. It means that the amount of fluid in the fracture is small compared to the amount of fluid that leaks from the crack in the surrounding porous material. This is of course a simplification, but the foregoing comparisons with analytical models will show that within the restrictions of the leak-off regime, it is not important, as opposed to what could be expected in a general case.

2.3. Hydro-mechanical coupling

In the lattice description, fluid flow is described in a lattice that is dual to the mechanical one. It follows the boundaries of the Voronoï polygons, the mechanical response being captured by the Delauney triangulation (figure 2).

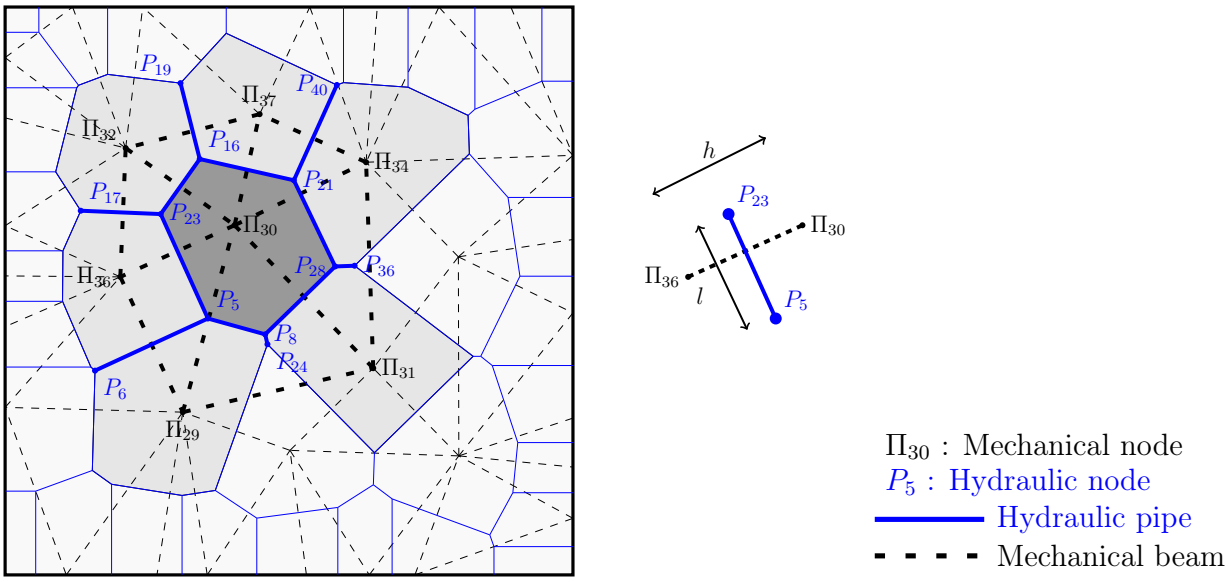

Figure 2: Dual hydro-mechanical lattice description. Only nodes at the vicinity of polyhedron Π_{30} are represented.

Each element of the hydraulic model (hydraulic pipe on Fig. 2) represents a one-dimensional flow between two nodes and has the following geometrical properties : the length of the pipe is l, the width of the pipe is h, corresponding to the length of the dual mechanical element, and the cross section of the pipe, A_h, equal to $h \times 1\text{m}$ in two dimension.

The corresponding conductivity matrix is given by equation (19).

$$\mathbf{K_h} = \frac{k}{\rho g} A_h \frac{1}{l} \begin{bmatrix} 1 & -1 \\ -1 & 1 \end{bmatrix} \tag{19}$$

In the mechanical model, polyhedron equilibrium is solved taking into account the total stress σ, that is the effective stress to which is added the contribution of the fluid:

$$\sigma = (1-\omega)\mathbf{D}_e\varepsilon + b\frac{P_i + P_j}{2}(1,0,0)^T \tag{20}$$

where $\frac{P_i+P_j}{2}$ represents the mean pressure in the hydraulic element.

In the hydraulic model, the local conductivity of the pipe, which drives the hydraulic pressure gradient, depends on the crack opening ω_c of the dual mechanical element considering a cubic law. The conductivity matrix is modified following equation (21)

$$\mathbf{K_h} = \left(\frac{\kappa}{\mu} + \frac{1}{h}\frac{\omega_c^3}{12\mu}\right) A\frac{1}{l}\begin{bmatrix} 1 & -1 \\ -1 & 1 \end{bmatrix} \tag{21}$$

This is a classical modification to the hydraulic conductivity matrix that assumes laminar flow in the pipe. Numerical coupling is achieved with a staggered scheme.

3. Comparisons with analytical solutions

3.1. Crack propagation regimes

Hydraulic fracturing is a coupled process that depends on the type of rock in which the crack is going to propagate and also on the properties of the fluid. Classicaly, energy dissipation has two sources: fracture propagation - the so-called toughness controlled regime, and fluid flow - the so-called viscosity controlled regime. This distinction holds for a hydraulically driven crack into an elastic material. When a hydraulically stimulated crack propagates within a permeable medium, its extend depends on the so-called *leak-off*, the quantity of fluid which drives out within the matrix and is not used for the propagation of the crack. Carter's model represents the leak-off as an unidimensional diffusive flow perpendicular to the crack lips (see e.g. ref. [28]). It follows that four regimes of crack propagation can be considered: Two toughness controlled regimes in the presence of small or large leak-off respectively, and two viscosity controlled regimes, again in the presence of small or large leak-off respectively.

In order to distinguish the toughness controlled regime from the viscosity controlled one, a non-dimensional viscosity is calculated [5]:

$$\mathscr{M} = f\left(Q_0, E, K, \mu\right) = \mu' \frac{Q_0 E'^3}{K'^4} \tag{22}$$

with

$$E' = \frac{E}{1-\nu^2} \quad \mu' = 12\mu \quad K' = 4\sqrt{\frac{2}{\pi}} K_{Ic} \tag{23}$$

where μ is the dynamic viscosity of the fluid and Q_0 is the fluid flux. If $\mathscr{M} \gg 1$ crack propagation follows the viscosity dominated regime and if $\mathscr{M} \ll 1$, it is the toughness dominated regime that is at stake.

The effect of the leak-off is illustrated with the help of Carter's coefficient:

$$C_L = \sqrt{\frac{\kappa}{\pi M \mu}} p \tag{24}$$

where κ is the permeability of the porous material, M is the Biot modulus, and p is the fluid pressure.

3.2. Analytical comparison for a permeable medium - toughness dominated regime

We consider here the analytical solution due to Bunger et al. [5] for a leak-off and toughness dominated crack propagation under hydraulic stimulation. The foregoing results have been summarized in Ref.[24], we provide here a complete presentation of them.

The geometry presented in Fig. 3 with a permeable medium is considered. Note that the analytical solution is based on brittle fracture. In order to describe a straight crack in the lattice model, the crack-path has been pre-meshed so as to avoid any bias due to the tortuosity of the crack path that may be obseved in an arbitrary lattice. The foregoing comparison is based on the model parameters used in Ref. [7] where a FEM approach with cohesive fracture is validated against the same analytical solution.

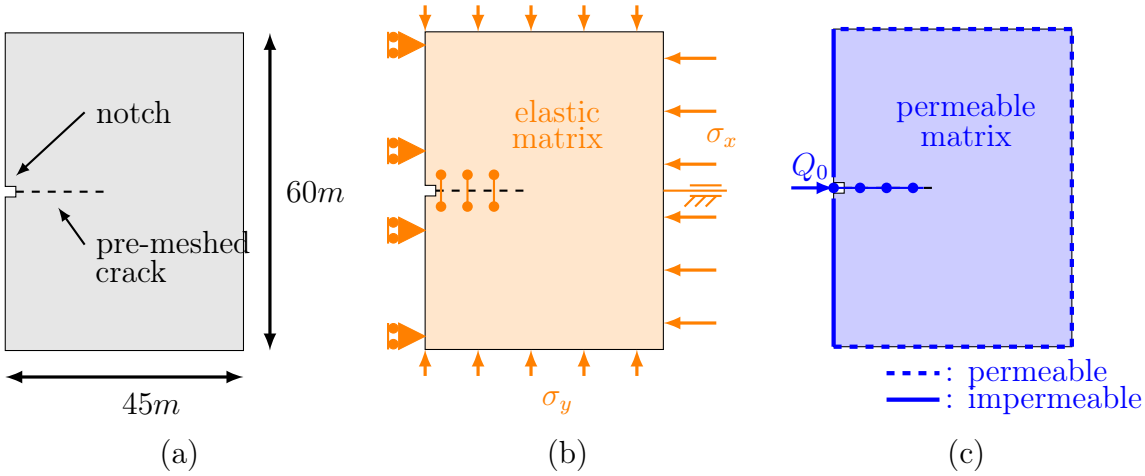

Figure 3: Comparison for a crack in a permeable medium : (a) geometry; (b)-(c) mechanical and hydraulic boundary conditions.

Poromechanical parameters are given in table 1. Minimal distance between nodes, d_{min}, is equal to 5cm. The time step in the staggered scheme is $\Delta t = 0.05$s. The fluid flow imposed is equal to 5×10^{-4} m^3/s. Confining stresses are $\sigma_x = 7$MPa and $\sigma_y = 5$MPa.

Parameter	**Unit**	**Symb.**	Matrix	Notch	Pre-meshed crack
Local Young modulus	[GPa]	E	23	17	17
Ratio E_s/E_n	[-]	γ	0.33	0.33	0.33
Damage threshold	[-]	$\varepsilon_{0,l}$	-	1×10^{-6}	74×10^{-6}
G_f parameter	[m]	ω_f	-	95×10^{-6}	95×10^{-6}
Ratio f_c/f_t	-	c	-	10^3	10^3
Ratio f_s/f_t	-	q	-	10^3	10^3
Biot's coefficient	[-]	b	0.75	0.75	0.75
Poromechanical modulus	[MPa]	M	68.7	68.7	68.7
Permeability	[m^2]	κ	3.47 10^{-17}	10^{-18}	10^{-18}
Fluid's dynamic viscosity	[Pa.s]	μ	0.0001	0.0001	0.0001
Fluid's volumetric mass	[kg/m^3]	ρ	1000	1000	1000
Initial crack opening	[mm]	$w_{\mathrm{c,ini}}$	0	5	0

Table 1: Parameters considered for the comparison with the analytical solution for a leak-off & toughness dominated regime.

With these parameters, Carter's coefficient is equal to $200 \times 10^{-6}\mathrm{m}\sqrt{\mathrm{s}}$, and the fracture propagation evolves in the leak-off and toughness dominated regime ($\mathcal{M} = 0,015 \ll 1$).

Figure 4 presents the comparison between the analytical solution and the lattice results in term of crack extend evolution with time and crack opening repartition.

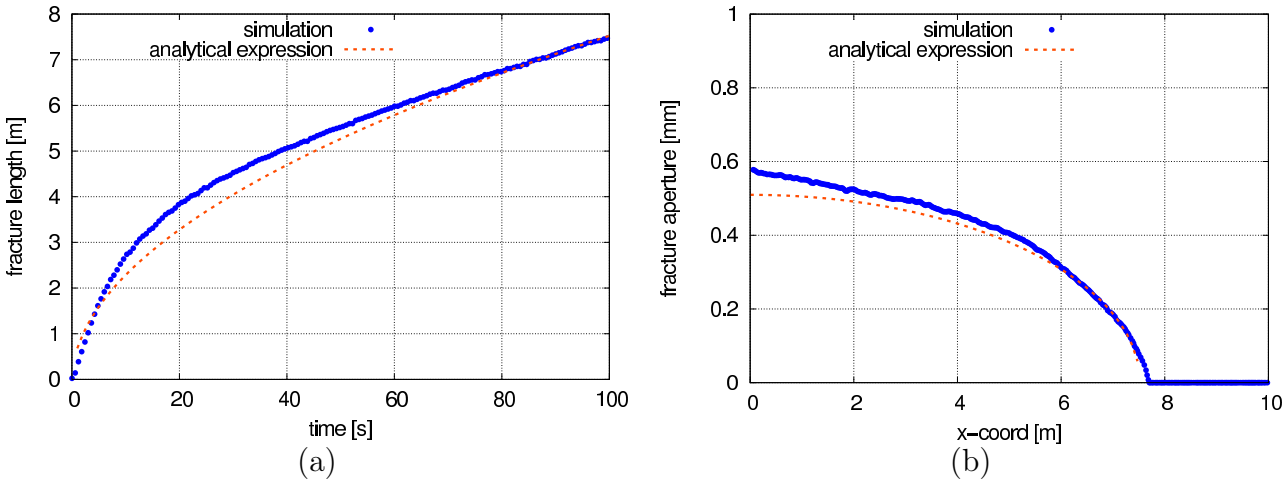

Figure 4: Comparison between the lattice results and an analytical solution for a leak-off & toughness dominated hydraulic fracture ([5]) : (a) crack extend evolution with time; (b) crack opening/aperture repartition at $t = 100s$ (reproduced from Ref.[24]).

A good agreement is observed, both on the history of crack propagation and on the crack

opening.

3.3. Analytical comparison for a permeable medium - viscosity dominated regime

We use here the solution due to Adachi and Detournay [1] related to a leak-off and viscosity dominated regime. The model geometry and parameters are the same as in the previous comparison, except for the dynamic viscosity $\mu = 0.1$Pa.s, the confining stresses $\sigma_x = 8$MPa and $\sigma_y = 7.2$MPa, and the permeability $\kappa = 1.07\ 10^{-14}\text{m}^2$. With these parameters, Carter's coefficient is equal to $1.6 \times 10^{-4}\text{m}\sqrt{\text{s}}$, and the fracture propagation evolves in the leak-off and viscosity dominated regime ($\mathcal{M} = 7.1 \gg 1$).

Figure 5 presents the comparison between the analytical solution and the lattice results in term of crack growth with time. Again, a reasonable agreement is observed.

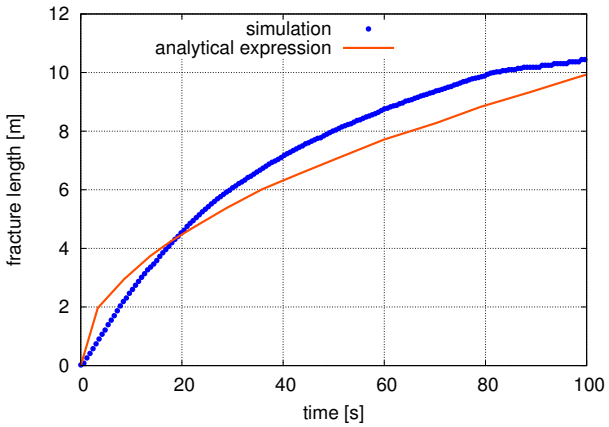

Figure 5: Comparison between the lattice results and an analytical solution for a leak-off & viscosity dominated hydraulic fracture [1] : crack extend evolution with time.

4. Influence of a joint on the hydraulic fracture crack path

The above model provides rather consistent predictions of hydraulic fracturing, at least in the regimes of crack propagation considered above. We may now advance to the case where a crack (i.e. a damage band in the present model) meets with an existing joint. The issues at stake are the description of the geometry of the joint in the lattice model and the poromechanical constitutive relations of the joint.

4.1. Implementation of a joint in the lattice model

Straight joints of finite length may be quite easily inserted in the lattice model (Figure 6). They are discretised into aligned nodal points that are placed on both side of the joint at an arbitrary small distance apart. It follows from Voronoi Tesselation and Delanunay triangulation that a lattice element is placed in between these nodes, perpendicular to the joint surface. These are the lattice elements that will follow the joint mechanical constitutive relation. Additional diagonal lattice elements connect nodes that do not face each other on the joint surface but their cross section is negligible and they do not contribute to the

mechanical response. In the dual hydraulic lattice, the pipes that describe the joint follows from Voronoi tesselation and the hydraulic characteristics of the joint will be assigned to these pipes.

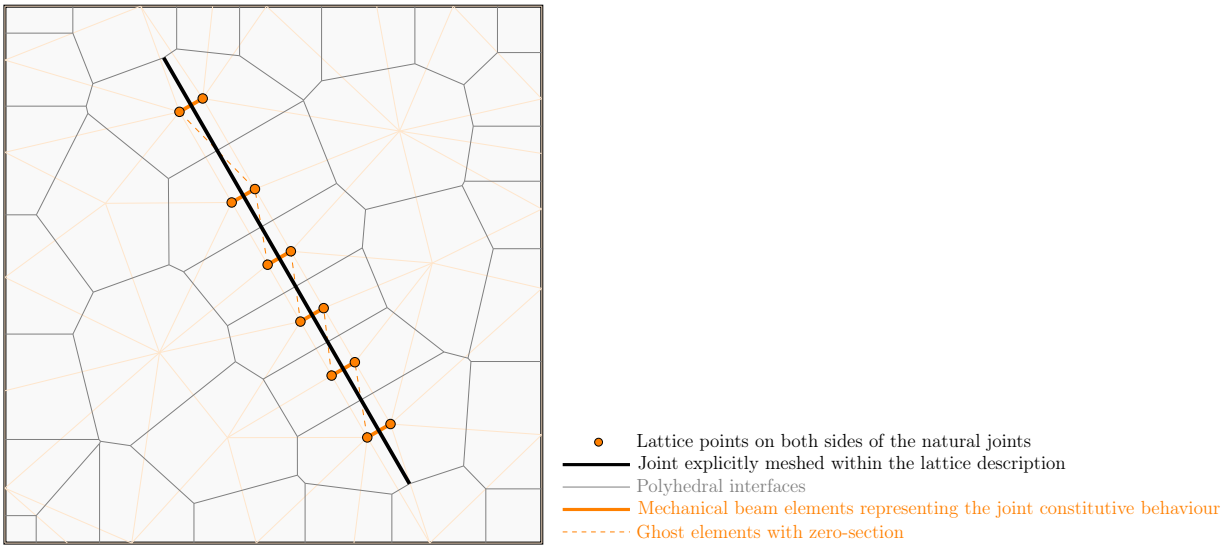

Figure 6: Lattice description of a 30^o inclined natural joint of finite length.

4.2. Constitutive model for the joint

The mechanical behaviour of the joint corresponds to the mechanical response of the lattice elements located perpendicularly to the joint as illustrated in Fig. 7. Here, it is going to be based upon an elasto-plastic model coupled to damage.

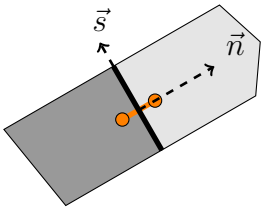

Figure 7: Lattice element describing a joint in its local coodinate system ($\vec{n}$,$\vec{s}$).

In the joint, the incremental deformation is the sum of the elastic and plastic ones:

$$d\varepsilon_{n,t} = d\varepsilon^E_{n,t} + d\varepsilon^P_{n,t} \tag{25a}$$

$$d\varepsilon_{s,t} = d\varepsilon^E_{s,t} + d\varepsilon^P_{s,t} \tag{25b}$$

where $d\varepsilon_{n,t}$ is the incremental normal deformation, $d\varepsilon_{s,t}$ is the incremental shear deformation, $d\varepsilon^E_{n,t}$ is the normal incremental elastic deformation, $d\varepsilon^E_{s,t}$ is the shear incremental elastic

deformation, $d\varepsilon^P_{n,t}$ is the increment of plastic normal strain, and $d\varepsilon^P_{s,t}$ is the increment of shear plastic deformation. Total stresses are related to the elastic strains as follow:

$$\sigma_{n,t} = E_n \varepsilon^E_{n,t} \tag{26a}$$

$$\sigma_{s,t} = E_s \varepsilon^E_{s,t} \tag{26b}$$

where E_n and E_s are the secant normal and shear stiffness of the joint, and $\sigma_{n,t}$ and $\sigma_{s,t}$ are the total normal and shear stresses respectively.

The evolution of the plastic strains is coupled to the growth of damage in the joint: in tension, the joint follows a normal stress-normal strain response that is similar to bulk rock (Eq. 10). As opposed to the description of rocks in the bulk, damage is not isotropic however in the sense that the normal stress v.s. normal strain response if affected by damage only.

$$E_n = (1-d)E_{n0}, \;\; E_s = constant \tag{27}$$

where d is the damage variable attached to the joint and E_{n0} is the normal elastic stifness of the cohesive joint, prior to any degradation.

As for the plastic response, it is governed by a Mohr Coulomb criterion that is modified so as to be expressed in term of the true stresses applied to the joint (in the continuum damage modelling sense).

$$f_{MC} = |\sigma_{s,t}| + \frac{\sigma_{n,t}}{1-d} tan(\phi) - c \tag{28}$$

with

$$c = c_0(1-d) + c_{res} \tag{29}$$

In these equations, c is the cohesion, and c_{res} is the residual cohesion after the joint has been totally damaged. ϕ is the friction angle which is assumed to be constant, whatever the value of damage. The evolution of the plastic strains follows the classical equations of non associated plasticity. The incremental normal plastic strain is related to the incremental shear plastic strain according to the equation:

$$d\varepsilon^P_{n,t} = |d\varepsilon^P_{s,t}| tan(\mu^j) \tag{30}$$

where μ^j is the dilatancy of the joint.

The equations that control the growth of damage account for two mechanism: (1) in tension, the response of the joint should exhibit almost no plastic strain as it is essentially due to the decohesion of the joint; (2) when the joint is subjected to shear loads, damage may occur also, but in this case it ought to be related to plastic strains. The evolution of damage given in Eqs. (11, 12) for the rock mass are modified for the joint in order to account for the effect of plastic strains:

$$f_d(\varepsilon^E, \varepsilon^P, \kappa^d) = \varepsilon_{eq} - \max(\kappa^d, \varepsilon_0) \tag{31a}$$

$$\varepsilon_{eq} = \left[\langle \varepsilon_n^E \rangle_+ + \alpha \sqrt{\varepsilon_n^{P2} + \varepsilon_s^{P2}}) \right] \tag{31b}$$

where ε_{eq} is the new equivalent deformation calculated accounting for both the elastic strains and plastic strains, $\langle \varepsilon_n^E \rangle_+$ is the positive part of the elastic deformation, and α is a model parameter that provides the influence of the plastic deformation on damage.

In tension - compression the response of the joint is very similar to that of rock in the bulk (with specific joint parameters). In simple shear, as shown in Fig. (8), the response of the joint exhibits first a plateau which is the classical Mohr Coulomb response (without hardening), then damage starts and strain softening occurs, until the residual cohesion has been reached asymptotically. In this calculation, the elastic stiffness of the joint is 4.4 Gpa, the shear stiffness is 1.45 GPa, $c = 1.4$ MPa and $c_{res} = 0.7$ MPa, $\phi = 30^o$, $\mu^j = 37^o$, and $\alpha = 0.2$.

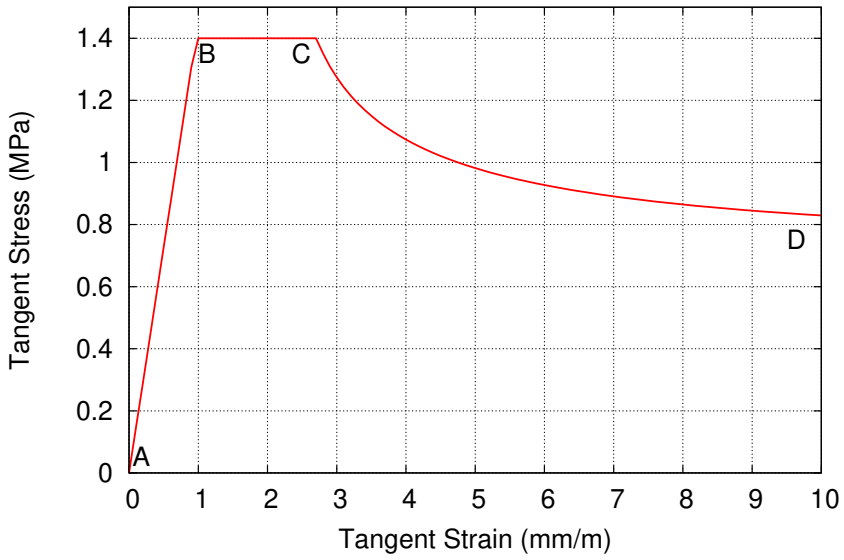

Figure 8: Response of the joint in simple shear

As illustrated in Ref. [24], this constitutive relation for the joint fits quite well with experimental data that have been performed on synthetic cohesive joints made of plaster (see Figure 9). In this specific case, it is possible to calibrate the model from experiments by testing joints with different inclinations with respect to the applied loads. Parameter α, which controls the amount of damage due to plastic strains, can be obtained from calibration of such experiments.

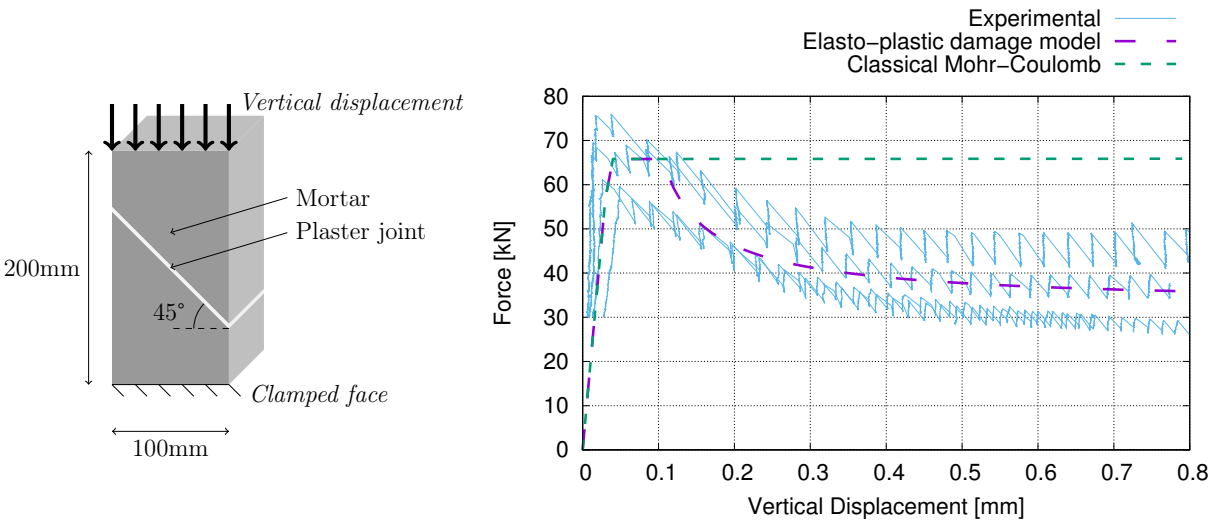

Figure 9: Comparison between experimental and numerical results for an indirect shear test (reproduced from Ref. [24]).

Finally, the implementation of this model does not carry any specific difficulties compared to standard constitutive relations where damage is coupled to plasticity. The fact that damage has been inserted in the constitutive relations adds, however, some complexity and it may be important to check if there is some added value to such as addition.

4.3. Crack-joint interaction in the mechanical problem

We consider here the following mechanical problem of a crack propagating in a notched square plate Fig. (10). The length of the notch is 0.05 m. At a distance of 0.1 m from the tip of the notch, a joint is placed vertically. The length of the joint is 0.2 m and its thickness is 0.001 mm. The center of the joint is aligned with the tip of the notch on the horizontal axis. Fig. (10-b) shows the boundary conditions of the problem. On the left vertical face of the square, horizontal displacements are fixed so as to represent an axis of symmetry. A constant vertical pressure is applied on the faces of the notch. Calculations are run by increasing this pressure step by step. The solid is modelled with lattice elements with a refined zone that encompasses the notch, the joint and the expected zone of crack propagation.

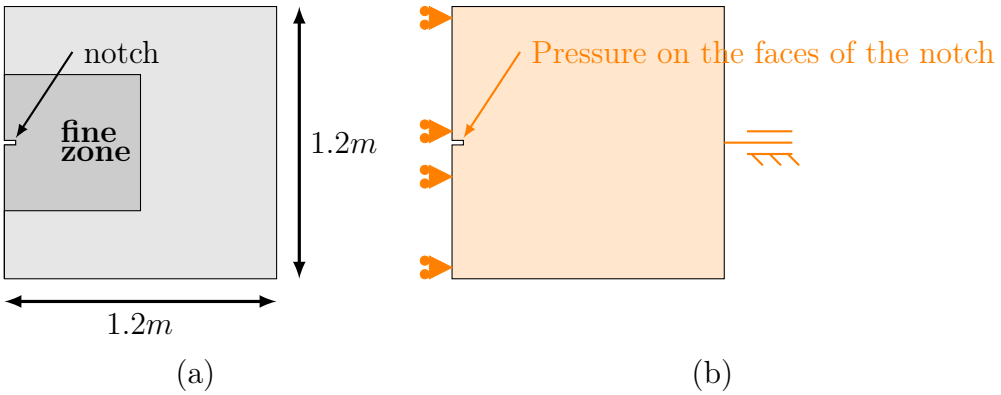

Figure 10: Interaction between a crack and a joint: (a) problem geometry, (b) boundary conditions

The model parameters are given in table 2.

Parameter	**Unit**	**Symb.**	Joint	Rock
Young's modulus	[GPa]	E	4.4	53
Ratio E_s/E_n	[-]	γ_1	0.33	0.33
Damage threshold	[-]	$\varepsilon_{0,l}$	$43,6 \times 10^{-6}$	275×10^{-6}
Control parameter for G_f	[m]	ω_f	150×10^{-6}	150×10^{-6}
Ratio f_c/f_t	[-]	c	–	10
Ratio f_s/f_t	[-]	q	–	2
Initial cohesion	[MPa]	c	$1,4$	-
Residual cohesion	[MPa]	c_{res}	$0,7$	-
Friction angle	[°]	ϕ	30	-
Dilatancy angle	[°]	μ^j	0	-
Influence of plasticity on damage	[-]	α	1%	-

Table 2: Model paratemers for the mechanical test case

Calculations have been performed with a Mohr Coulomb elastic perfectly plastic model for the joint and with the present damage plasticity model. The mechanical model for the rock is kept the same. The parameters in the perfectly plastic model are those of the joint, with damage set to be equal to zero. The results are very similar until the crack passes the joint.

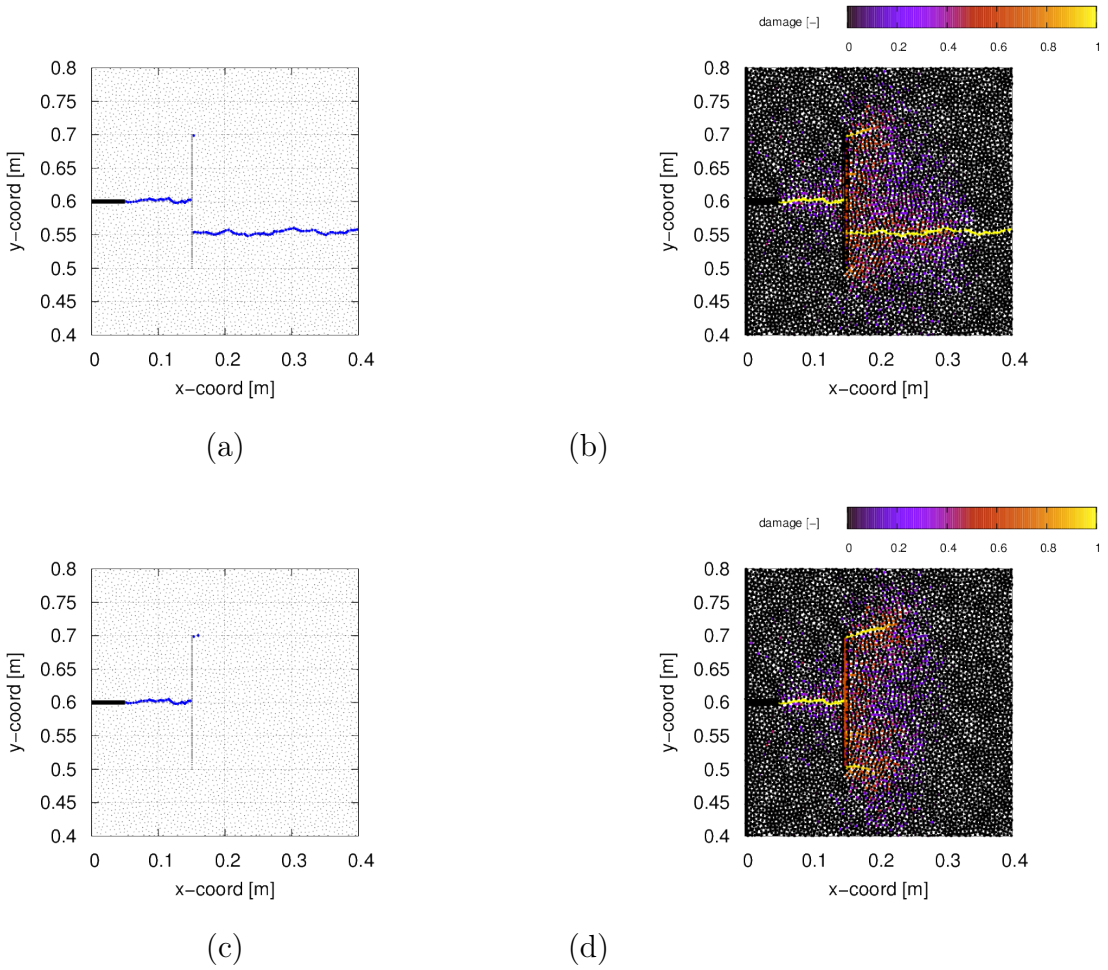

Figure 11: Mechanical problem: Crack propagation and interaction with a vertical joint: (a) perfect plasticity - crack path, (b) perfect plasticity - damage map, (c) damage plastic model - crack path, (d) damage plastic model - damage map. The crack path is defined as the elements where damage is above 0.99.

Fig.11 shows the crack paths and damage zones obtained for the two problems at a pressure of 76 MPa. First, the crack is stopped upon reaching the joint. The difference between the two calculations is what happens next. For a perfectly plastic joint, the crack passes through the joint eventually (Fig.11-a), whereas it propagates from one of the tip of the joint when a coupled damage-plastic model is implemented (Fig.11-c). In both cases, the damage maps show that damage develops nearby the tips of the joint, but the final crack maps are very different. This difference is due to the cohesion of the joint compared the mechanical properties of the rock. If the cohesion is not degraded, and if it is sufficiently high compared to the mechanical properties of the rocks, the crack will pass through the joint. If it is degraded due to damage, the joint acts as a screen and stresses are transferred to the tip of the joint. The two calculations have been performed with the same discretisation,

therefore, it should not have any influence on this difference.

This example shows that the interaction between a propagating crack and an existing joint in a rock mass depends on the constitutive model that is implemented. In practice, it is rather difficult to measure experimentally the mechanical response of joints in order to be able to discriminate several constitutive models and to calibrate model parameters. Such joints may not even be accessible for observation and sampling. Therefore, one should be very cautious when analysing computations as their result may severely depend on quantities that are quite uncertain. Sensitivity analyses on the type of joint models and their parameters, at least, should be performed in order to get access to the variety of possible results considering this uncertainty.

4.4. Crack-joint interaction in the hydromechanical problem

We consider now the same problem but instead of a mechanical distributed load applied on the faces of the notch, we look for the effect of a pressurized fluid. The hydraulic response of the joint follows exactly the same equations as for the bulk rock (i.e. the variation of permeability due to damage), with different model parameters however.

We have studied two configurations: in the first one, the joint is vertical and in the second one the joint is inclined with an angle of 45^o degrees. The mechanical model for the joint is the coupled damage-plasticity one.

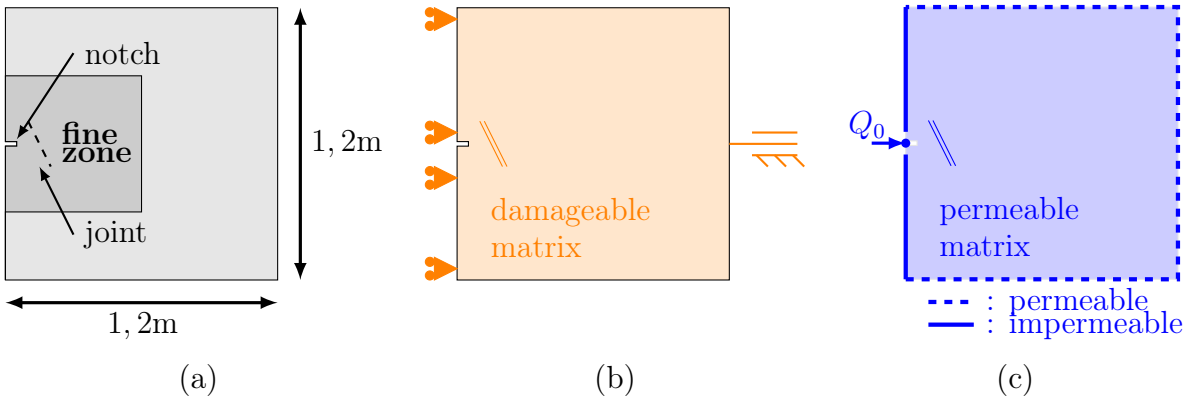

Figure 12: Influence of a natural joint on the hydraulic fracture crack path : (a) geometry; (b)-(c) mechanical and hydraulic boundary conditions.

The model parameters are provided in table 3. The hydraulic response of the joint is exactly the same as that of the rock, but with a different initial permeability. These parameters are consistent with a leak-off and toughness dominated regime. The time step of the staggered scheme is Δt =0.02 s. The fluid flow imposed is equal to 50×10^{-6} m^3/s.

Parameter	**Unit**	**Symb.**	Joint	Matrix
Young's modulus	[GPa]	E	4.4	53
Ratio E_s/E_n	[-]	γ_1	0.33	0.33
Damage threshold	[-]	$\varepsilon_{0,l}$	43.6×10^{-6}	275×10^{-6}
G_f parameter	[m]	ω_f	150×10^{-6}	150×10^{-6}
Ratio f_c/f_t	[-]	c	–	10
Ratio f_s/f_t	[-]	q	–	2
Cohesion	[MPa]	c	1.4	-
Friction angle	[°]	ϕ	30	-
Dilatancy	[°]	μ^j	0	-
Biot's coefficient	[-]	b	$1,0$	$1,0$
Permeability	[m^2]	κ	10^{-12}	3.45×10^{-17}
Biot's modulus	[MPa]	M	68.7	68.7
Fluid's dynamic viscosity	[Pa.s]	μ	10^{-4}	10^{-4}
Fluid's volumetric mass	[kg/m^3]	ρ	1000	1000

Table 3: Influence of a natural joint on the hydraulic fracture crack path : mechanical and hydraulic parameters.

Figs 13 and 14 show the damage maps, the maps of fluid pressure, and the distributions of plastic strains in the joint for the two configurations plotted at the end of the calculation (time = 100s).

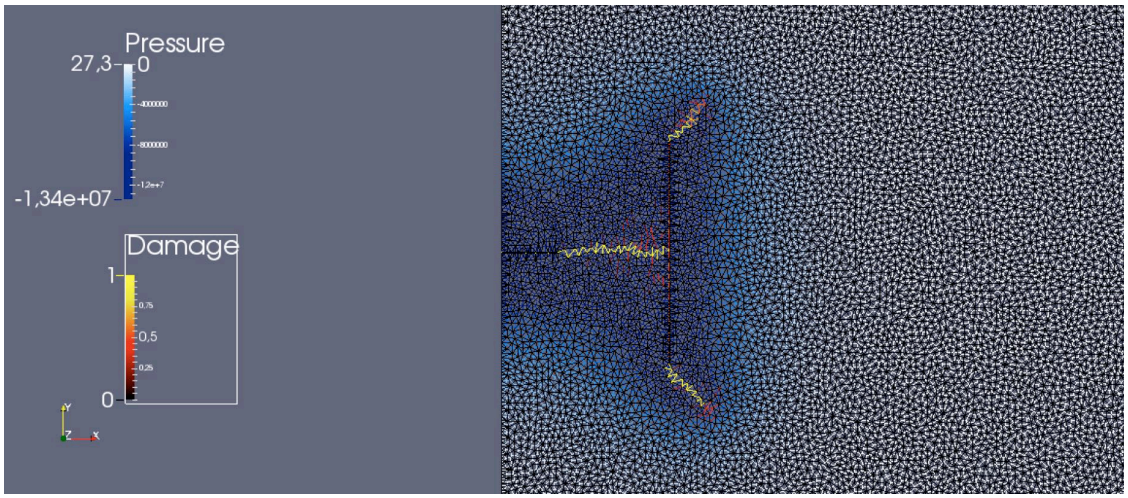

(a)

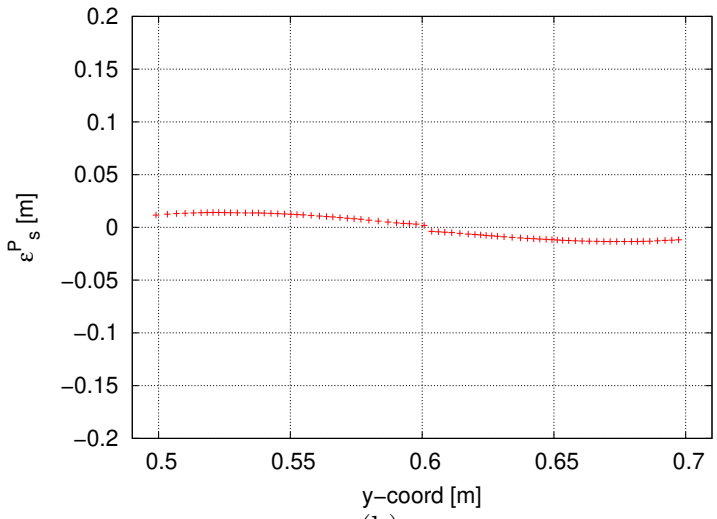

(b)

Figure 13: Vertical joint, time = 100s: (a) maps of damage and fluid pressure, (b) tangent plastic deformations in the joint.

In both cases, the crack does not passes through the joint because the cohesion of the joint is not sufficiently high compared to the mechanical properties of the rock. As shown in Figs.13-(b) and 14-(b), plastic strains develop in the joint due to shear. Due to the plastic strains and to the fluid pressure, damage grows inside the joint. As a consequence, the permeability of the joint increases, which is is a signature of the reactivation of the joint.

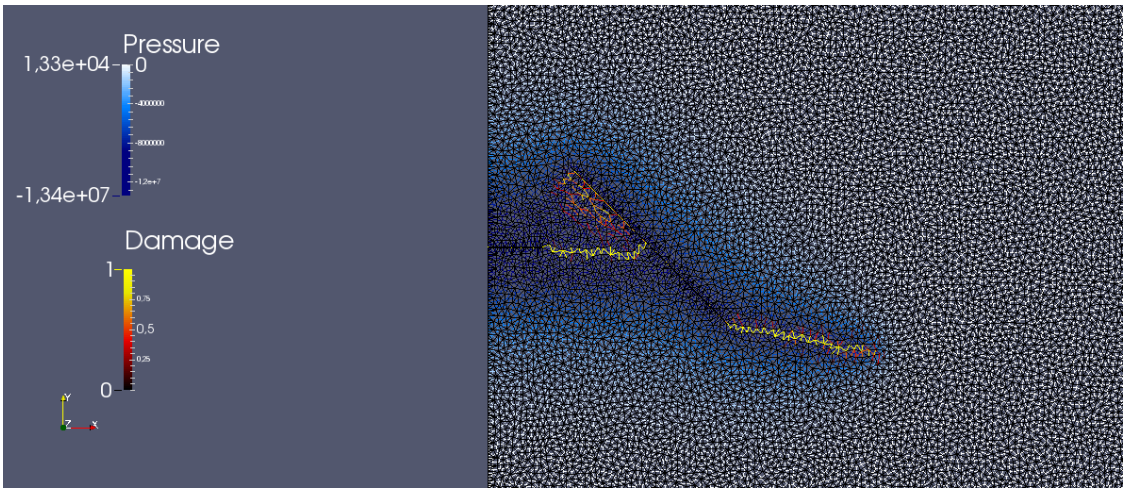

(a)

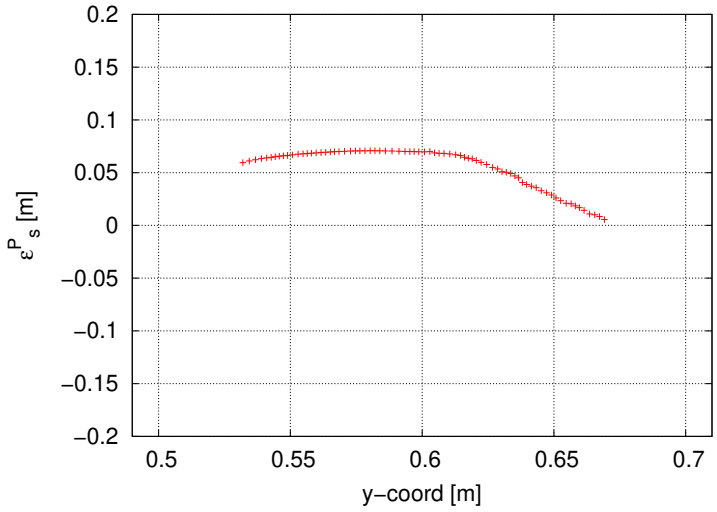

(b)

Figure 14: Inclined joint, time = 100s: (a) (a) maps of damage and fluid pressure, (b) tangent plastic deformations in the joint.

This jump in fluid pressure is shown in Fig. (15). The jump is greater for the vertical notch than for the inclined joint. For the vertical joint, the drop corresponds to the filling of the joint with fluid, yielding a decohesion due to the growing fluid pressure with little plastic strains. During this process, the crack is arrested. Fluid injection yields a subsequent increase of pressure. Then, damage occurs at both tips of the joint, as if the two where independent. One will take over eventually due to local differences in the lattice discretisation (which is not symmetric). For the inclined joint, this process is more smooth and plastic strains in the joint are more intense. Damage in the joint develops mostly due to these plastic strains. One may observe on the damage map that diffuse damage occurs below the upper part of the joint, in between the joint and the crack (see Fig.14-a). This

tensile damage is due to positive strains induced by Poisson's effect in the rock mass. In practice, such an extend of damage is useful to promote the production of fluid from the hydraulically driven fracture as it increases the size of the so-called stimulated volume.

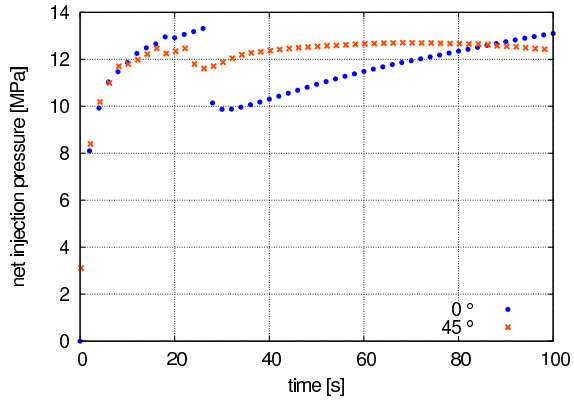

Figure 15: History of the fluid injection pressure in the two joint configurations (vertical and inclined).

5. Conclusions

A hydro-mechanical coupled lattice-based model has been presented for the simulation of crack propagation induced by fluid injection in rocks containing cohesive joints. Rock follows an isotropic damage model for tensile fracture and cohesive joints follow a coupled plasticity-damage model. The cohesion of the joint is decreased due to damage controlled by both elastic normal strains and plastic strains. As for the hydraulic part, permeability increases upon damage following a cubic law, in the joint and in the rock.

The discretisation is performed according to a dual lattice approach, a Delanay triangulation for the solid and the boundaries of the associated Voronoï tesselation for the hydraulic part. We use a poromechanical framework for porous materials saturated with a single fluid. Computations are performed with a staggered scheme. 2D examples have been presented.

The capability of the hydro-mechanical model at describing hydraulically driven fracture has been tested against analytical models available in the literature. Comparisons cover both the viscosity and toughness dominated regimes, under the assumption that leak-off prevails over the storage capacity of the fluid in the fracture. A very good agreement is found with theoretical solutions.

Then, the interaction between a propagating crack and an existing joint has been analysed. Two configurations have been considered: the case of a joint that is orthogonal to the crack path and the case of a joint that is inclined by 45^o with respect to the crack path. For the vertical joint, the crack is first arrested because the cohesive joint is weaker than the rock mass. Then, it reinitiates at both crack tips. For the inclined joint, the crack follows the joint and therefore its path is deviated. Damage in the rock develops in the back of the crack tip, thereby enhancing the increase of permeability due to damage in the rock mass.

This framework, however, needs to be compared with experimental data, with the intrinsic difficulty of accessing to the model parameters for joints presents in rock masses. In practice, the influence of the crack propagation to the mechanical parameters of the joint and the relatively high uncertainty for these parameters call for sensitivity studies, from which sets of potential crack paths could be obtained.

6. Acknowledgements

This study has been performed under a collaboration with Total E&P and with the support from the Pyrennées Atlantiques District. It has been also partially supported by the Investissement d'Avenir French programme (ANR-16-IDEX-0002) under the framework of the E2S UPPA hub Newpores.

References

[1] Adachi, J., Detournay, E., 2008. Plane strain propagation of a hydraulic fracture in a permeable rock. Engineering Fracture Mechanics 75, 4666–4694.

[2] Asahina, D.,Houseworth, J.E., Birkholzer, J.T., Rutqvist, J., Bolander, J.E., 2014. Hydro-mechanical model for wetting/drying and fracture development in geomaterials. Computers and Geosciences, 65, 15–23.

[3] Asahina, D.,Pan, P., Tsusaka, K., Tajeda, M., Bolander, J.E., 2017. Simulating hydraulic fracturing processes in laboratory-scale geological media using three-dimensional TOUGH-RBSN. Journal of Rock Mechanics and Geotechnical Engineering, 10, 1102–1111.

[4] de Borst, R., 2017. Fluid Flow in Fractured and Fracturing Porous Media: A Unified View. Mechanics Research Communications, 80, 47–57.

[5] Bunger, A., Detournay, E., Garagash, D., 2005. Toughness-dominated hydraulic fracture with leak-off. International Journal of Fracture 134, 175–190.

[6] Cao, T.D.,Milanese, E., Remij, E.W.,Rizzato, P., Remmers, J.J.C.,Simoni, L., Huyghe, J.M.,Hussain, F.,Schreffler, B.A., 2017. Interaction between crack tip advancement and fluid flow in fracturing saturated porous media. Mechanics Research Communications, 80, 24–37.

[7] Carrier, B.,Granet, S., 2012. Numerical modeling of hydraulic fracture problem in permeable medium using cohesive zone model. Engineering Fracture Mechanics, 79, 312–328.

[8] Chatzigeorgiou, G.,Picandet, V., Khelidj, A., Pijaudier-Cabot, G., 2005. Coupling Between Progressive Damage and Permeability of Concrete: Analysis with a Discrete Model. nt. J. Num. Anal. Meths. in Geomechanics, 29, 1005–1018.

[9] Chau, V-T.,Bazant, Z.P..,Su, Y., 2016. Growth Model for Large Branched Three-Dimensional Hydraulic Crack System in Gas or Oil Shale. Phil. Trans. R. Soc. A, 374, 20150418

[10] Chen, W., Maurel, O., Reess, T., De Ferron, A., La Borderie, C., Pijaudier-Cabot, G., Rey-Bethbeder, F., Jacques, A., 2012. Experimental study on an alternative oil stimulation technique for tight gas reservoirs based on dynamic shock waves generated by Pulsed Arc Electrohydraulic Discharges. Journal of Petroleum Science and Engineering, 88-89, 67–74.

[11] Cipolla, C., Warpinski, N., Mayerhofer, M., Lolon, E., Vincent, M., 2010. The Relationship Between Fracture Complexity, Reservoir Properties, and Fracture-Treatment Design. SPE Production & Operations 25, 1–25.

[12] Coussy, O., 2004. Poromechanics. John Wiley.

[13] Economides, M., Nolte, K., 2000. Reservoir Stimulation. John Wiley & Sons Ltd, West Sussex, England.

[14] Engelder, T., Lash, G., Uzcátegui, R., 2009. Joint sets that enhance production from Middle and Upper Devonian gas shales of the Appalachian Basin. AAPG Bulletin 93, 857–889.

[15] Fu, P.,Johnson, S.M.,Carrigan, C.R., 2013. An Explicit Coupled Hydro-Geomechanical Model for Simulating Hydraulic Fracturing in Arbitrary Discrete Fracture Networks. Int. J. Numerical and Analytical Methods in Geomechanics , 37, 2278–2300.
[16] Gale, J., Reed, R., Holder, J., 2007. Natural fractures in the Barnett Shale and their importance for hydraulic fracture treatments. AAPG Bulletin 91, 603–622.
[17] Geertsma, J., De Klerk, F., 1969. A Rapid Method of Predicting Width and Extent of Hydraulically Induced Fractures. Journal of Petroleum Technology, 21, 1571–1581.
[18] Geertsma, J., Haafkens, R., 1979. A Comparison of the Theories for Predicting Width and Extent of Vertical Hydraulically Induced Fractures. Journal of Energy Resources Technology, 101, 8.
[19] Grassl, P., Fahy, C., Gallipoli, D., Wheeler, S.J., 2015. On a 2D hydro-mechanical lattice approach for modelling hydraulic fracture. Journal of the Mechanics and Physics of Solids, 75, 104–118.
[20] Grassl, P., Grégoire, D., Rojas-Solano, L., Pijaudier-Cabot, G., 2012. Meso-scale modelling of the size effect on the fracture process zone of concrete. International Journal of Solids and Structures, 49, 1818–1827.
[21] Grassl, P., Jirásek, M., 2010. Meso-scale approach to modelling the fracture process zone of concrete subjected to uniaxial tension. International Journal of Solids and Structures, 47, 957–968.
[22] Grassl, P.,Bolander, J.E., 2016. Three-Dimensional Network Model for Coupling of Fracture and Mass Transport in Quasi-Brittle Geomaterials. Materials, 9, 782.
[23] Grégoire, D., Verdon, L., Lefort, V., Grassl, P., Saliba, J., Regoin, J., Loukili, A., Pijaudier-Cabot, G., 2015. Mesoscale analysis of failure in quasi-brittle materials: comparison between lattice model and acoustic emission data. International Journal for Numerical and Analytical Methods in Geomechanics, 39, 1639–1664.
[24] Gregoire, D.,Lefort, V., Nouailletas, O.,Pijaudier-Cabot, G., 2016. 2D-Lattice Modelling of Crack Propagation Induced by Fluid Injection in Heterogeneous Quasi-Brittle Solids. Procedia Structural Integrity, 2, 2698–2705.
[25] Hattori, G., Trevelyan, J.,Augarde, C.E., Coombs, W.M.,Aplin, A.C., 2017. Numerical Simulation of Fracking in Shale Rocks: Current State and Future Approach. Arch. Computat. Methods Eng., 24, 281–317.
[26] He, M.,Hutchinson, J.W., 1989. Crack Deflection at an Interface between Dissimilar Elastic Materials. Int. J. Solids and Structures, 25, 1053–1067.
[27] Heider, Y.,Markett, B., 2017. A Phase-Field Modeling Approach of Hydraulic Fracture in Saturated Porous Media. Mechanics Research Communications, 80, 38–46.
[28] Howard, G., Fast, C.R., 1957. Optimum Fluid Characteristics for Fracture Extension. Proceedings of the American Petroleum Institute, 261–270.
[29] Khristianovic, S., Zheltov, Y., 1955. Khristianovic, S.A., Zheltov, Y.P., in: 4th World Petroleum Congress, Carlo Colombo, Rome., Rome. pp. 579–586.
[30] King, G., 2010. Thirty years of gas-shale fracturing: What have we learned? JPT Journal of Petroleum Technology, 62, 88–90.
[31] Lecampion, B., Desroches, J., 2015. Simultaneous initiation and growth of multiple radial hydraulic fractures from a horizontal wellbore. Journal of the Mechanics and Physics of Solids, 82, 235–258.
[32] Lecampion, B.,Bunger, A., Zhang, X., 2018. Numerical methods for hydraulic fracture propagation: A review of recent trends. Journal of Natural Gas Science and Engineering, 49, 66–83.
[33] Lefort, V., Pijaudier-Cabot, G., Grégoire, D., 2015. Analysis by Ripley's function of the correlations involved during failure in quasi-brittle materials: Experimental and numerical investigations at the mesoscale. Engineering Fracture Mechanics, 147, 449–467.
[34] Li, W.,Zhou, X., Carey, J.W., Frash, L.P., Cusatis, G., 2018. Multiphysics Lattice Discrete Particle Modeling (M-LDPM) for the Simulation of Shale Fracture Permeability. Rock Mechanics and Rock Engineering, 51, 12, 25-10-2018.
[35] Mauthe, S.,Miehe, C., 2017. Hydraulic Fracture in Poro-Hydro-Elastic Media. Mechanics Research Communications, 80, 69–83.
[36] Meriaux, C., Lister, J.R.,Lyakowsky, V., Amon, A., 1999. Dyke Propagation with Distributed Damage

of Host Rock. Earth and Planetary Science Letters, 165, 177–185.
[37] Milanese, E.,Yilmaz, O., Molinari, J.F., Schreffler, B.A., 2016. Avalanches in dry and saturated disordered media at fracture. Physical Review E, 93, 043002.
[38] Milanese, E.,Yilmaz, O., Molinari, J.F., Schreffler, B.A., 2017. Avalanches in dry and saturated disordered media at fracture in shear and mixed mode scenarios. Mechanics Research Communications, 80, 58–68.
[39] Nikolic, M., 2015. Rock mechanics, failure phenomena with pre-existing cracks and internal fluid flow through cracks. These de l'Ecole Normale Superieure de Cachan, Cachan, France.
[40] Nordgren, R., 1972. Propagation of a Vertical Hydraulic Fracture. Society of Petroleum Engineers Journal, 12, 306–314.
[41] Papachristos, E.,Scholtes, L., Donze, F.V., Chareyre, B., 2017. Intensity and volumetric characterizations of hydraulically driven fractures by hydro-mechanical simulations. International Journal of Rock Mechanics and Mining Sciences, 93, 163–178.
[42] Perkins, T.K., L. R. Kern, 1961. Widths of Hydraulic Fractures. Journal of Petroleum Technology, 13, 937 – 949.
[43] Rahimi-Aghdam, S., Chau, V-T.,Lee, H., Nguyen, H..,Li, W., Karra, S., Rougier, E.,Viswanathan, H., Srinivasan, G..,Bazant, Z.P.., 2019. Branching of Hydraulic Cracks Enabling Permeability of Gas or Oil Shale with Closed Natural Fractures. Proc. National Adademy of Sciences, 116, 1532–1537.
[44] Rezakhani, R.,Zhou, X., Cusatis, G., 2017. A multiscale framework for the simulation of the anisotropic mechanical behavior of shale. Int. J. Numerical and Analytical Methods in Geomechanics, 41, 1494–1522.
[45] Shi, F.,Wang, X., Liu, C.,Liu, H., Wu, H., 2017. An XFEM-based method with reduction technique for modeling hydraulic fracture propagation in formations containing frictional natural fractures. Engineering Frat. mech., 173, 64–90.
[46] Sobhaniaragh, B., Nguyen, V.P.,Mansur, W.J., Peters, F.C., 2018. Pore Pressure and Stress Coupling in Closely-Spaced Hydraulic Fracturing Designs on Adjacent Horizontal Wellbores. European Journal of Mechanics A/Solids, 67, 18–33.
[47] Slowik, V., Saouma, V.E., 2000. Water Pressure in Propagating Concrete Cracks. Journal of Structural Engineering ASCE, February, 235–242.
[48] Tzschichholz F.,Herrmann H., 1995. Simulations of pressure fluctuations and acoustic emission in hydraulic fracturing. Physical Review E Statistical Physics Plasmas Fluids and Related Interdisciplinary Topics, 51, 1961–1970.
[49] Warpinski, N., Teufel, L., 1987. Influence of Geologic Discontinuities on Hydraulic Fracture Propagation. Journal of Petroleum Technology, 209–220.
[50] Zeng, X.,Wei, Y., 2017. Crack Deflection in Brittle Media with Heterogeneous Interfaces and its Application in Shale Fracking. J. Mech. Phys. Solids, 101, 235–249.